Self-organized flocking in mobile robot swarms

4 authors, including:

Ali Emre Turgut
KU Leuven
32 PUBLICATIONS   734 CITATIONS

SEE PROFILE

Hande Çelikkanat
Middle East Technical University
20 PUBLICATIONS   324 CITATIONS

SEE PROFILE

Erol Sahin
Middle East Technical University
96 PUBLICATIONS   2,901 CITATIONS

SEE PROFILE

Some of the authors of this publication are also working on these related projects:

Swarm robotics View project

Collective motion in robotics View project

Self-organized flocking in mobile robot swarms

**Ali E. Turgut · Hande Çelikkanat · Fatih Gökçe ·
Erol Şahin**

Abstract In this paper, we study self-organized flocking in a swarm of mobile robots. We
present Kobot, a mobile robot platform developed specifically for swarm robotic studies.
We describe its infrared-based short range sensing system, capable of measuring the dis-
tance from obstacles and detecting kin robots, and a novel sensing system called the virtual
heading system (VHS) which uses a digital compass and a wireless communication module
for sensing the relative headings of neighboring robots.

We propose a behavior based on heading alignment and proximal control that is capa-
ble of generating self-organized flocking in a swarm of Kobots. By self-organized flocking
we mean that a swarm of mobile robots, initially connected via proximal sensing, is able
to wander in an environment by moving as a coherent group in open space and to avoid
obstacles as if it were a "super-organism". We propose a number of metrics to evaluate the
quality of flocking. We use a default set of behavioral parameter values that can generate
acceptable flocking in robots, and analyze the sensitivity of the flocking behavior against
changes in each of the parameters using the metrics that were proposed. We show that the
proposed behavior can generate flocking in a small group of physical robots in a closed
arena as well as in a swarm of 1000 simulated robots in open space. We vary the three main
characteristics of the VHS, namely: (1) the amount and nature of noise in the measurement

A.E. Turgut · H. Çelikkanat · F. Gökçe · E. Şahin (✉)
Kovan Research Lab., Dept. of Computer Eng., Middle East Technical University, Ankara, Turkey
e-mail: erol@ceng.metu.edu.tr

A.E. Turgut
e-mail: aturgut@ceng.metu.edu.tr

H. Çelikkanat
e-mail: hande@ceng.metu.edu.tr

F. Gökçe
e-mail: fgokce@ceng.metu.edu.tr

of heading, (2) the number of VHS neighbors, and (3) the range of wireless communication. Our experiments show that the range of communication is the main factor that determines the maximum number of robots that can flock together and that the behavior is highly robust against the other two VHS characteristics. We conclude by discussing this result in the light of related theoretical studies in statistical physics.

Keywords Swarm robotics · Self-organization · Flocking

1 Introduction

Flocking, the coherent maneuvering of a group of individuals in space as if they were a super-organism, is a widely observed phenomenon in animal societies. Flocks of birds, herds of quadrupeds and schools of fish are often shown as fascinating examples of self-organized coordination (Camazine et al. 2001; Okubo 1986; Parrish et al. 2002). Biological studies (Ballerini et al. 2008; Pitcher and Parrish 1993; Simpson et al. 2006) indicate that, through flocking, individuals gain a number of advantages that increase their survival rate. First, individuals in a flock have reduced chances of being captured by predators, since through collective sensing individuals can sense approaching predators more easily, and as a large group they may warn off an attacking predator to deflect its attack away from the group (Partridge 1982). Also by traveling together, the individuals reduce the probability of detection by predators. Second, it has been argued (Kruszelnicki 2008; Simons 2004) that during migration, flocks of birds or schools of fish can follow migration routes in a more precise and robust way through collective sensing. Third, flocking can improve energy efficiency during the travel. For example, migrating birds are known to utilize the stream-lines formed by their frontal neighbors to increase their flying ranges (Ballerini et al. 2008; Kruszelnicki 2008).

In artificial swarms, Reynolds (1987) was the first to demonstrate that flocking, which he described as a "general class of polarized, non-colliding, aggregate motion" of a group of individuals, can be created. Being interested in obtaining a realistic looking flocking behavior in computer animations, Reynolds assumed that the individuals can sense the bearing, range, and orientation of their neighbors and showed that flocking can be achieved using three simple behaviors: namely *collision avoidance*, *velocity matching,* and *flock centering*. Roughly speaking, the first behavior keeps the individuals away from each other avoiding collisions, the second aims to match the velocity of an individual with its neighbors, and the third forces an individual to stay close to its neighbors.

1.1 Previous work

In one of the earliest attempts towards obtaining flocking in a group of robots, Matarić (1994) combined a set of "basic behaviors": safe-wandering, aggregation, dispersion, and homing. In this study, the robots were able to sense the obstacles in the environment, localize themselves with respect to a set of stationary beacons and broadcast the position information to the other robots in the group. The flocking behavior developed can be seen as collective homing, where a homing direction is known and the robots try to stay together while moving. Through the utilization of the safe-wandering behavior the robots were also shown to be able to avoid obstacles on the path towards the goal.

Kelly and Keating (1996) used a group of 10 robots, that were able to sense the obstacles in close proximity using ultrasonic sensors, and the relative range and bearing of neighbor-

ing robots through the use of a custom-made infrared (IR) system. The robots used wireless communication to elect a leader for the flock. The leader would then wander in the environment and the others would follow. The IR system was used to generate attractive forces towards other robots whereas the ultrasonic sensors generated repulsive forces from other robots and obstacles.

Hayes and Dormiani-Tabatabaei (2002) proposed a "leaderless distributed flocking algorithm that is more conducive to implementation on embodied agents" than the ones being used in computer animation. The flocking behavior consisted of two simple behaviors, namely collision avoidance and velocity matching flock centering. It was assumed that the robots were able to sense the range and bearing of their neighbors within a predefined sensing range. Using this information each robot would compute the center-of-mass (CoM) of the group based on the relative position of its neighbors and the heading towards a predefined goal area. The CoM was then used to implement flock cohesion, and the change in CoM at each time step was used to align the robot with the group. The authors implemented the proposed algorithm on the Webots simulator and optimized the parameters of the algorithm, which were then verified using a group of 10 robots. In the experiments with physical robots, however, the authors had to "emulate the range and bearing sensor signals" by tracking the robots using an overhead camera system and broadcasting these readings to the robots.

Campo et al. (2006) presented a method for the self-organized negotiation of goal direction for a group of robots to cooperatively transport a heavy object to a nest located at an estimated position. The robots negotiate their estimation of the location of the nest through an omni-directional vision system and announce their own estimations of the nest by forming a specific pattern of colored LEDs surrounding their body. They perceive their peers' estimations and align to a common estimation of the nest, which improves the individual estimations greatly.

Nembrini et al. (2002) developed a set of behaviors that use wireless connectivity among robots to achieve aggregation, collective obstacle avoidance, and collective taxis towards a beacon. The behaviors were tested on a swarm of seven robots that were equipped with a set of IR sensors for obstacle detection, an omni-directional IR system for robot detection and a wireless communication system. Although the behaviors were shown to be robust and scalable in simulated experiments, the authors reported limited success with physical robots blaming the insufficiency of the hardware for the failure in maintenance of coherence (Nembrini 2005).

Despite the interest in flocking, self-organized flocking as observed in nature has still not been achieved in robotics. The few experimental studies in robotics reviewed above either used a virtual or an explicit leader (Kelly and Keating 1996) to lead a group of individuals, or they assumed that a goal heading (or area) is sensed by the whole group (Campo et al. 2006; Hayes and Dormiani-Tabatabaei 2002; Matarić 1994; Nembrini 2005). Moreover, in some of the studies (Hayes and Dormiani-Tabatabaei 2002; Regmi et al. 2005), the authors had to resort to using "emulated" sensors. Studies that propose using vision to control flocking (Moshtagh et al. 2006), although promising, still remain to be implemented and evaluated on physical robots. Hence, swarm robotic systems that can maneuver in an environment as a "super-organism" and avoid obstacles on their path as a flock do not exist yet.

The main reason behind this failure, as partially discussed above, is that the flocking behaviors proposed and studied in other domains, such as computer graphics, statistical physics, and control theory, assume that the individuals can sense the relative position and bearing of their neighbors on an individual basis. Such sensing abilities are still not available

on most available robot platforms, with Kelly and Keatings' (1996) custom active IR system and Campo et al.'s (2006) heading negotiation mechanism being two exceptions. The proximity sensors on most mobile robots, such as ultrasound and IR-based systems, can sense only the range to the closest point of a neighboring robot, and multiple range readings can be returned from a close neighboring robot. Furthermore, the sensing of bearing, velocity, and orientation of neighboring robots are still difficult with off-the-shelf sensors available on robots. Hence, there exists a major gap between studies that propose flocking behaviors in simulation and studies on real robots.

In this paper, we study the self-organized flocking of a swarm of mobile robots. By self-organized flocking, we mean that a swarm of mobile robots, initially connected through proximal sensing, should be able to wander in an environment as if it were a "super-organism" by moving as a coherent group in open space and avoiding obstacles in the environment. Different from other robotic flocking studies, the challenge of self-organized flocking as studied in this paper lies in developing a fully decentralized and scalable coordination method. Behaviors that include the use of a designated or elected leader within the group, or the use of a common goal/homing direction, are excluded.

2 The Kobot robot platform

In this study, we use a mobile robot platform (Turgut et al. 2007) specifically designed for swarm robotic studies, called Kobot, and shown in Fig. 1(a). The robot has the size of a CD (diameter of 12 cm), a weight of 350 grams, and it is differentially driven by two high quality DC motors. It has eight IR sensors for kin and obstacle detection and a digital compass for heading measurement. An IEEE 802.15.4/ZigBee compliant XBee wireless module with a range of approximately 20 m indoors is used for communication between robots and between the robots and a computer console. The robot hosts a 20 MHz PIC18F4620A microcontroller, which provides a control step duration of 110 ms. The microcontroller can be
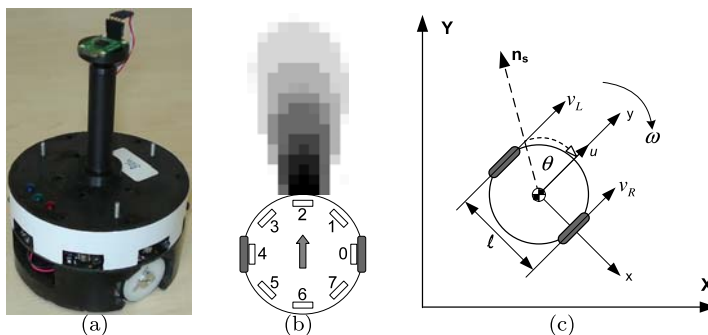

Fig. 1 (**a**) Photo of a Kobot. (**b**) The scaled sketch. The *circle* represents the body. The *small rectangles* show the placement of the IR sensors placed evenly at multiples of 45° around the body. Each *square* patch in the *gray* scale blob indicates the output of the sensor averaged over 200 samples. A white plastic stick with a diameter of 2 cm is used as the target. Darker colors denote higher values of sensor measurement. (**c**) The reference frame is fixed to the center of the robot where the x-axis coincides with the rotation axis of the wheels. The forward velocity (u) is along the y-axis. ω denotes the angular velocity of the robot. v_R and v_L denote the velocities of the *right* and *left* motors, respectively. The y-axis of the body-fixed reference frame makes an angle of θ with the *sensed North* direction (n_s) at the instant the figure is drawn which is the current heading of the robot. l is the distance between the wheels

programmed through a wireless communication link. The low-power design of its systems lets Kobot operate for 10 hours with a 2000 mAh Li-Poly battery.

2.1 Infrared short-range sensing system

The infrared short-range sensing system (IRSS) is designed for proximal sensing. The IRSS can distinguish kin-robots and obstacles within a range of approximately 20 cm at seven discrete levels at 18 Hz. The use of modulated IR signals minimizes environmental interference. Figure 1(b) illustrates the placement of 8 sensing modules each of which has an IR LED with a half-cone angle of 25°, a modulated IR receiver and a microcontroller.

Crosstalk among the nearby robots is avoided using the CSMA-CA (carrier sense multiple access collision avoidance) algorithm during sensing. The measurement cycle of the IR sensor starts with the command of a coordinator microcontroller telling the sensors to wait for a random period of time to look for any IR signal, which indicates the presence of a nearby kin-robot. The measurement is initiated only when the sensor does not receive any modulated IR signals for a certain period of time. The measurement is performed by varying the power of the IR LED to determine the minimum level at which an object is detected. The kth sensor returns an integer pair (o_k, r_k), where $o_k \in \{0, 1, \ldots, 7\}$ denotes the detection level to the object being sensed ($o_k = 1$ and $o_k = 7$ indicate, respectively, a far and nearby object, whereas $o_k = 0$ stands for no detection), and $r_k \in \{0, 1\}$ indicates whether the sensed object is an obstacle or a kin robot.

2.2 Virtual heading sensor

The *virtual heading sensor* (VHS) uses a digital compass and a wireless communication module to sense the relative orientations of the neighboring robots. The VHS measures the heading of the robot (θ) in clockwise direction with respect to the *sensed North,* as shown in Fig. 1(c), and broadcasts it to the neighboring robots within its communication range at each control step.

The hard-iron effect[1] may cause the sensed North to deviate from the absolute North. However, we assume that the sensed North remains approximately the same within the range of communication of the robots and that the heading values broadcasted can be considered to be on the same coordinate frame allowing the robots to detect their relative headings with respect to each other. In our experiments, we observed that this type of sensing is quite robust even in indoor environments where metal objects are abundant.

3 Characteristics and modeling of the sensors

We developed a physics-based simulator, called Controllable-Swarm Simulator (CoSS) and shown in Fig. 2(b), using the ODE (Open Dynamics Engine) physics engine to study flocking behavior with a large group of robots. The body and wheels of the Kobot are modeled as cylinders. The DC motors are simulated using virtual motorized hinge joints and the virtual weights of the components are adjusted to obtain a similar movement pattern with similar motor torques. The characteristics and modeling of the IRSS and VHS are developed through systematic experiments as described below.

---

[1]The hard-iron effect is a local change in the magnetic field lines of the Earth near a ferrous metal or a permanent magnet, which results in a deviation of the sensed North direction of a compass from the absolute North at that point.

Fig. 2 (**a**) A photo of 7 Kobots. (**b**) A screenshot from CoSS

3.1 Modeling of the infrared short-range sensing system

We conducted two systematic experiments to characterize the proximal sensing and kin-detection of Kobots. In both experiments, a robot is placed at the origin of the reference coordinate frame and the second robot is placed along a 25×25 grid with 1 cm spacing, as sketched in Fig. 3(a). For each of the points, 200 readings of (o_k, r_k) coming from the 2nd sensor (frontal sensor) of the robot placed at the origin (see Fig. 1) are recorded. In the first experiment, referred to as the obstacle experiment, the IRSS of the second robot remains turned off, acting merely as a circular obstacle. In the second experiment, referred to as the robot experiment, the IRSS of the second robot is turned on, creating IR interference on the IRSS of the first robot.

Figure 3(b) plots the data obtained from the obstacle experiment. The average o_k values shown as gray scale patches, indicate that the sensor has a range of approximately 8 cm and 20 cm along the lateral and the longitudinal axis, respectively. The same data for the robot experiment is plotted in Fig. 3(d). The Pearson product-moment correlation coefficient (Dalgaard 2004) (ρ) between the proximity measurements of the obstacle and the robot experiments is calculated to be 0.99, proving that the proximal sensing is not affected by the active sensors of another robot. The robot detection performance is plotted in Fig. 3(c) where the gray scale patches encode the rate of success. The plot shows that kin-robots can be detected with almost 100% success through most of the operating range of the sensor, indicating that the disturbance caused by the crosstalk of the active sensors is minimal.

The data obtained from these experiments are used to simulate the sensing characteristics of the IRSS using the sampling technique (Miglino et al. 1995). However, it should be noted that these experiments model the sensing characteristics of the IRSS for circular obstacles and robots, only. The sensing of environmental objects, such as planar walls and corners, has not yet been modeled, and simulation of Kobots is only utilized to study flocking in open space.

3.2 Modeling of the virtual heading sensor

The virtual heading sensor can be characterized by three parameters; namely (1) the range of wireless communication, (2) the number of neighboring robots that can be "heard", referred to as *VHS neighbors* in the rest of the paper, and (3) the nature and amount of noise of the digital compass. Within the context of this study, the first two parameters are not independent. The number of VHS neighbors (N_c) depends on the range of communication (R), the
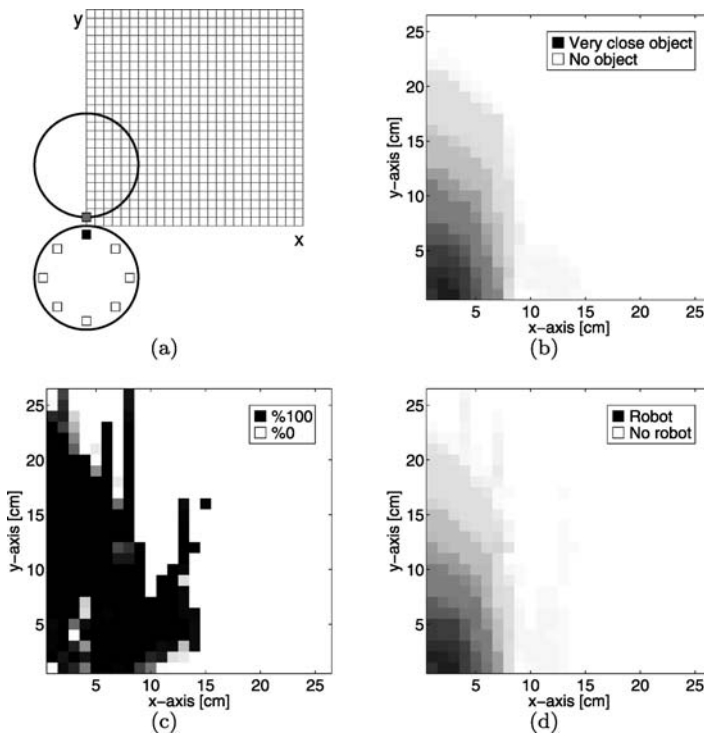
Fig. 3 (**a**) The experimental setup. The *circle* at the *lower left* corner represents the robot used to make the sensing measurements. Samples are collected from the 2nd (frontal sensor) while the other sensors are also turned on. The *upper circle* indicates the second robot that was used as an obstacle (with its IRSS being turned off) or as a robot (with its IRSS being turned on). (**b**) The obstacle experiment. (**c**) Success rate in robot detection. (**d**) The robot experiment. Darker colors in (**b**) and (**d**) denote a nearby obstacle or robot, respectively

density of the robots, and the frequency and duration of communication. In this paper, the density of the robots is usually determined by the inter-robot spacing during flocking; the frequency of communication is determined by the duration of the control step; and the duration of communication is determined by the limitations of the communication module. Both the inter-robot spacing during flocking and the frequency of communication are constrained by the physical implementation of Kobots. Therefore, we use the range of communication as a free parameter in our characterization.

Since the number of Kobots available is relatively small, we conduct the experiments using Prowler (Simon et al. 2003), an event-driven probabilistic wireless network simulator. We place 817 nodes on a hexagonal grid with 25 cm spacing (estimated inter-robot spacing during flocking), as shown in Fig. 4(a), and we measure N_c for the robot placed at the center of the swarm. Figure 4(b) plots the distribution of N_c values for different R values. It shows that N_c increases with R up to 24 and eventually saturates around 20. This is due to the increase in collisions of the heading messages when the range is wide.

The noise in the virtual heading sensor depends on the noise characteristics of the communication module and the digital compass. The communication module's operation is free of noise and the digital compass module has a noise of $\pm0.5°$ in ideal operating conditions where there is no nearby ferrous metal. However, in typical indoor environments ferrous
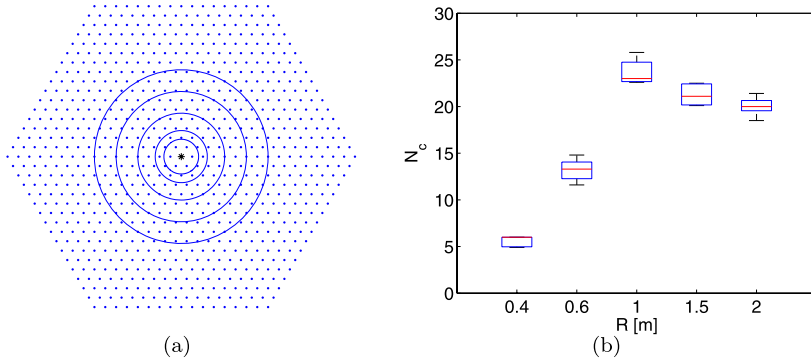
(a) (b)

Fig. 4 Range of communication experiments. (**a**) Topology of nodes. *Circles* indicate various communication ranges of the central node. (**b**) The distribution of N_c for the central node. In this figure and the subsequent box-plot figures, the ends of the boxes and the horizontal line in between correspond to the first and third quartiles and the median values, respectively. The top and bottom whiskers indicate the largest and smallest non-outlier data, respectively. The data in between the first and third quartiles lie within the 50% confidence interval, while the data in between the whiskers lie within the 99.3% confidence interval
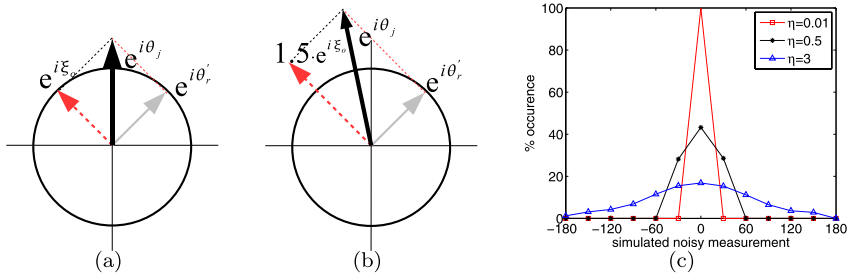

(a) (b) (c)

Fig. 5 (**a**, **b**) Vectorial noise model. The actual heading vector of the jth neighbor in the body-fixed reference frame ($e^{i\theta'_r}$) is denoted by a *gray arrow*. The noise vector ($e^{i\xi_o}$) is shown by a *dashed arrow* and the resultant vector ($e^{i\theta_j}$) is denoted by a *bold continuous arrow*. η is 1 in (**a**) and 1.5 in (**b**). Adapted from Baldassarre (2008). (**c**) Histogram of simulated noisy measurements of VHS

metals are abundant, and their existence can create large disturbances in the readings of the compass.

We treat the disturbances on the VHS as noise, and characterize it using the vectorial noise model (Gregoire et al. 2003). In this model, a random noise vector, characterized by a random direction and a constant magnitude, is added vectorially to each received heading vector, as illustrated in Figs. 5(a) and 5(b). The resulting noisy heading vector of the jth neighbor in the body-fixed reference frame is calculated as:

$$\theta_j = \angle\{e^{i\theta'_r} + \eta e^{i\xi_o}\}, \qquad (1)$$

where θ'_r is the actual heading of the jth neighbor in the body-fixed reference frame calculated as $\theta - \theta_r + \frac{\pi}{2}$. Here, θ_r is the received heading of the jth neighbor and θ is the robot's

own heading.[2] η is the magnitude of the noise vector that is regarded as a parameter, and ξ_o is its direction. $\angle(\cdot)$ calculates the argument of the resulting vector. ξ_o represents the noise and is chosen from a Gaussian distribution $N(\mu = \theta_r', \sigma)$, where μ and σ are the mean and the standard deviation, respectively.

In order to demonstrate the nature and the scale of disturbances in the heading readings, we simulated the proposed model. In our simulation, θ_r' is taken as 0 and the noise vector is assumed to have a distribution characterized by $N(\mu = \theta_r', \sigma = \pm\frac{\pi}{2})$. We varied η and for each value we simulated 10000 readings. Figure 5(c) plots the histogram of the noisy readings, indicating that the standard deviation of the resultant distribution is controlled by the value of η.

4 The flocking behavior

The flocking behavior consists of heading alignment and proximal control behaviors, combined in a weighted vector sum:

$$\mathbf{a} = \frac{\mathbf{h} + \beta \ \mathbf{p}}{\|\mathbf{h} + \beta \ \mathbf{p}\|},$$

(2)

where $\mathbf{h}$ is the heading alignment vector, $\mathbf{p}$ is the proximal control vector having a weight of β, and $\mathbf{a}$ is the desired heading vector. $\|\cdot\|$ calculates the Euclidean norm of a given vector.

4.1 Heading alignment behavior

The heading alignment behavior aims to align the robot with the average heading of its neighbors. The VHS is used to receive the current headings of the neighbors. The alignment vector ($\mathbf{h}$) is then calculated as:

$$\mathbf{h} = \frac{\sum_{j \in \mathcal{N}_R} e^{i\theta_j}}{\| \sum_{j \in \mathcal{N}_R} e^{i\theta_j} \|},$$

where $\mathcal{N}_R$ denotes the set of VHS neighbors when the communication range of VHS is set to R. θ_j is the heading of the jth neighbor in the body-fixed reference frame (see (1)).

4.2 Proximal control behavior

The proximal control behavior uses readings obtained from the IRSS to (1) avoid collisions with robots and obstacles, and (2) maintain cohesion between the robots. When an obstacle or a robot is detected by an IR sensor, a virtual force proportional to the square of the deviation of the current detection level from the desired detection level, referred to as o_{des}, is applied to the robot. The virtual force, denoted by f_k, is defined as:

$$f_k = \begin{cases} -\frac{(o_k - o_{des})^2}{C} & \text{if } o_k \geq o_{des}, \\ \frac{(o_k - o_{des})^2}{C} & \text{otherwise}, \end{cases}$$

(3)

---

[2]The heading of the robot is the angle between the *sensed North* and the *y*-axis of its body-fixed reference frame in clockwise direction as shown in Fig. 1(c). $\frac{\pi}{2}$ is added to $\theta - \theta_r$ to obtain the heading of the jth neighbor in the body-fixed reference frame.

Fig. 6 The virtual force (f_k) is drawn with respect to o_k where o_{des} for robots is set to 3. Higher values of o_k indicate closer distances. The virtual force value always stays within $[-1, 1]$ regardless of the value of o_k
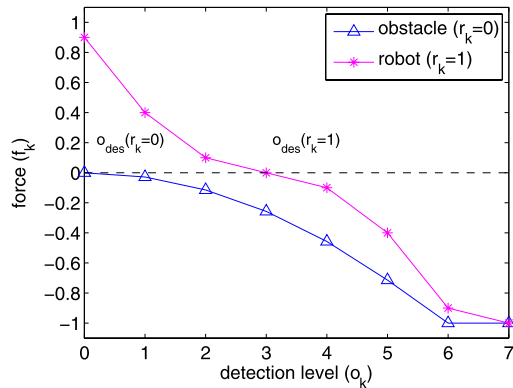
where C is a scaling constant. o_{des} is taken as a finite value for kin-robots, and 0 for obstacles (remember that o_k indicates the detection level and that $o_k = 1$ and $o_k = 7$ denote, respectively, a far and a very close obstacle/robot) forcing the flock to remain together as a coherent body while avoiding obstacles. Figure 6 plots f_k for both robots and obstacles where the o_{des} values for robots and obstacles are set to 3 and 0, respectively.

The calculation of the normalized proximal control vector, **p**, is as follows:

$$\mathbf{p} = \frac{1}{8} \sum_k f_k e^{i\phi_k}, \tag{4}$$

where $k \in \{0, 1, \ldots, 7\}$ denotes the sensor positioned at angle $\phi_k = \frac{\pi}{4}k$ with respect to the x-axis of the body-fixed reference frame (Fig. 1(b)).

4.3 Motion control

The desired heading vector, **a**, is used to calculate the forward (u) and angular (ω) velocities using (5) and (6), respectively. Specifically, u is calculated as:

$$u = \begin{cases} (\mathbf{a} \cdot \mathbf{a}_c)^\gamma \, u_{\max} & \text{if } \mathbf{a} \cdot \mathbf{a}_c \geq 0, \\ 0 & \text{otherwise,} \end{cases} \tag{5}$$

where $\mathbf{a}_c$ is the current heading vector of the robot coincident with the y-axis of the body-fixed reference frame (see Fig. 1(c)). γ is a parameter to enable ($\gamma = 1$) or disable ($\gamma = 0$) the modulation of the forward velocity.

The forward velocity of the robot is modulated by the "urge" to turn, as sketched in Fig. 7. The modulation is implemented as the dot product of the desired (**a**) and current heading (**a**$_c$) vectors. When the urge to turn is low, meaning that the robot is already moving in the desired direction, the forward velocity is allowed to achieve its maximum value ($u_{\max}$) as shown in Fig. 7(a). Conversely, when the urge to turn is high, u decreases, converging to 0 in the extreme case, where the robot only rotates around its center, as illustrated in Fig. 7(b). And when the dot product is negative, indicating that the angle between the two vectors is greater than 90°, as shown in Fig. 7(c), u is set to 0. In this case, the robot's motion is constrained to rotation only. Failure to do so would have resulted in robots moving backwards, a situation that would complicate the behavior and its analysis.
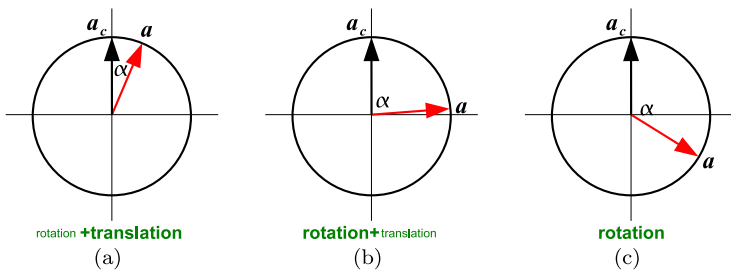
Fig. 7 Modulation of the forward velocity (u) when $\gamma = 1$. (**a**) The robot makes mostly translation. $\alpha \approx 0° \Rightarrow u \approx u_{\max}$. (**b**) The robot makes mostly rotation. $\alpha \approx 90° \Rightarrow u \approx 0$. (**c**) The robot makes only rotation. $\alpha > 90° \Rightarrow u = 0$

The angular velocity (ω) of the robot is controlled by a proportional controller using the deviation of the desired angle from the current direction of the robot:

$$\omega = (\angle \mathbf{a}_c - \angle \mathbf{a}) K_p, \tag{6}$$

where K_p is the proportionality constant of the controller.

The rotational speeds of the right and left motors (Fig. 1(c)) are eventually calculated as follows:

$$N_R = \left(u - \frac{\omega}{2} l \right) \frac{60}{2\pi r},$$

$$N_L = \left(u + \frac{\omega}{2} l \right) \frac{60}{2\pi r},$$

where N_R and N_L are the rotational speeds (rotations per minute) of the right and left motors, respectively, l is the distance between the wheels of the robot (meters), u is the forward velocity (meters per second), and ω is the angular velocity (radians per second).

5 Metrics of flocking behavior

There are no formal definitions for self-organized flocking in the literature. However, it is generally agreed that flocking individuals should be aligned towards a common direction, move as a compact, coherent and proximally connected group without collisions, and preferably in a smooth and fast way. In this section we describe a number of measures that can be used to evaluate these different aspects of flocking and describe how these measures are computed in our experiments.

(1) The *order* (ψ) measures the angular order of the robots (Vicsek et al. 1995):

$$\psi(t) = \frac{1}{N} \left| \sum_{k=1}^{N} e^{i\theta_k} \right|, \tag{7}$$

where N is the number of robots in the swarm and θ_k is the heading of the kth robot at time t.

The order is calculated by recording the heading values broadcasted by the robots at each control step. The order gets close to 1 when the swarm is aligned; in this case the system is said to be in an *ordered* state. However, when the swarm is unaligned, the order decreases to 0; in this case the system is said to be in a *disordered* state.

(2) The *entropy* (S) measures the positional disorder of the swarm (Balch 2000). It is calculated by finding every possible cluster via changing the maximum distance (h) between the individuals in a same cluster. Two robots i and j are considered to be in a same cluster if and only if $\|\mathbf{r}_i - \mathbf{r}_j\| \leq h$ holds, where $\mathbf{r}_i$ and $\mathbf{r}_j$ denote the position vectors of the ith and jth robots. Shannon's information entropy H(h) of a cluster with a maximum distance h is defined as:

$$\text{H}(h) = \sum_{k=1}^{M} p_k \log_2(p_k), \tag{8}$$

where p_k is the proportion of the individuals in the kth cluster and M is the number of clusters for a given h.

These entropy values are integrated over all possible h's ranging from 0 to ∞ to find the total entropy (S):

$$S = \int_0^\infty \text{H}(h) \, dh. \tag{9}$$

Figure 8 shows four possible configurations that a 7-robot swarm can attain. In (a), individuals are placed as a chain which is the least desired configuration having the highest entropy value. Considering configurations (b) and (c), the latter has a smaller entropy value since the individuals are closer to each other. Finally, the configuration in (d), which is the desired configuration, has the smallest entropy value since it is the most positionally ordered and optimally spaced configuration for a 7-robot swarm.

The entropy measure is unbounded and the desired entropy value is different for swarms of different sizes. Therefore, in our analysis, we use the rate of change in entropy, denoted by dS/dt as an indication of stability or instability of the flock. A positive dS/dt value at the end of a flocking experiment indicates an unstable swarm that is spreading apart in space, whereas a dS/dt that is approximately zero indicates a stable and coherent swarm.

The entropy is calculated from the relative positions of the robots using a moving overhead camera. The relative positions of the robots are determined by using the OpenCV computer vision library (Correll et al. 2006).

(3) The *swarm velocity* (V_G) is the average velocity of the geometric center of the swarm during the whole course of its motion. This metric is calculated by dividing the displacement of the geometric center of the swarm by the duration of flocking. A high swarm
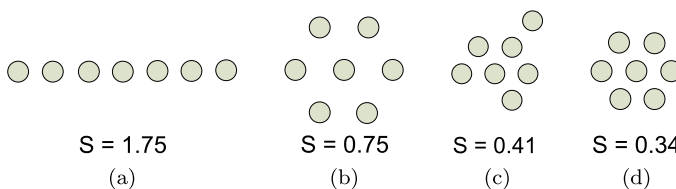

S = 1.75   S = 0.75   S = 0.41   S = 0.34

(a)   (b)   (c)   (d)

Fig. 8 Entropy values for four different configurations of a 7-robot swarm. The entropy decreases as the configuration becomes more compact

velocity indicates an efficiently and smoothly moving swarm, whereas a low swarm velocity is an indicator of inefficiency and jerkiness of motion.

(4) *Size of largest cluster* is the number of robots in the largest cluster that stays together during motion. It is an indication of how large a swarm can continue moving without being fragmented into smaller clusters.

Based on these metrics, we argue that desirable flocking requires: (1) a high value of order indicating alignment among individuals, (2) approximately constant entropy (dS/dt converging to zero) indicating a compact and coherent swarm, (3) high swarm velocity indicating coherent motion, and (4) a high value of the size of largest swarm indicating a larger swarm that can move together.

6 Sensitivity of the behavioral parameters

The flocking behavior has a number of parameters to be determined, namely: the weight of the proximal control vector (β), the proportional gain (K_p), the maximum forward speed ($u_{\max}$), the forward speed modulation (γ), and the desired detection level (o_{des}). Finding the optimal control parameters is a difficult optimization problem that we do not tackle in this study. Instead, we use a default set of parameters (listed in Table 1) that are known to generate acceptable flocking in Kobots and in CoSS, and analyze the sensitivity of the parameters to small changes.

In the experiments discussed below, we vary one behavioral parameter at a time and analyze the performance of flocking using some of the metrics defined in the previous section. This allows us both to understand how the different components of the behavior affect the overall behavior and to make a 1-D sensitivity analysis in the parameter space to show that the default parameter set is locally optimal.

The experiments are conducted both with small swarms using physical and simulated robots, and with large swarms simulated within CoSS. In the experiments on small swarms, we used 7 physical or simulated robots, whereas in experiments on large swarms we used

Table 1 The default parameter settings for the behavior and the VHS

Parameter	Default value
Behavior	
Weight of proximal control (β)	12 (for small swarms)
	4 (for large swarms)
Proportional gain for angular velocity (K_p)	0.5
Maximum forward speed ($u_{\max}$)	7 cm/s
Desired detection level (o_{des})	3
Modulation parameter for forward velocity (γ)	1
VHS	
Communication range (R)	20 m
Number of VHS neighbors (N_c)	20
Nature of noise (ξ_o)	$N(\mu = \theta_r', \sigma = \pm\frac{\pi}{2})$
Amount of noise (η)	3

100 simulated robots. In all experiments, the robots are initially positioned at random ori-
entations in a regular hexagonal formation with a 25 cm inter-robot distance to ensure co-
hesiveness. In each experiment within CoSS, unless otherwise stated, the simulations are
conducted for 1000 seconds. The experiments made with Kobots and CoSS are repeated 3
and 20 times, respectively. In our experiments, we calculated the average rate of change in
entropy (dS/dt) during the final 500 seconds of the CoSS experiments.

The experiments have shown that the same values for all but the β parameter generate
stable flocking for both small and large swarms.

6.1 Weight of the proximal control behavior

The β parameter determines the relative strength of the proximal control behavior in relation
to the heading alignment behavior. In our experiments, we vary β (0, 4, 8, 12, and 16) and
measure the rate of change of the entropy and the swarm velocity and try to determine the
value that maximizes the swarm velocity while ensuring coherence. The results of the ex-
periments conducted with 7 physical and simulated robots are plotted in Figs. 9(a) and 9(b),
whereas the results obtained from 100 simulated robots are plotted in Figs. 9(c) and 9(d).
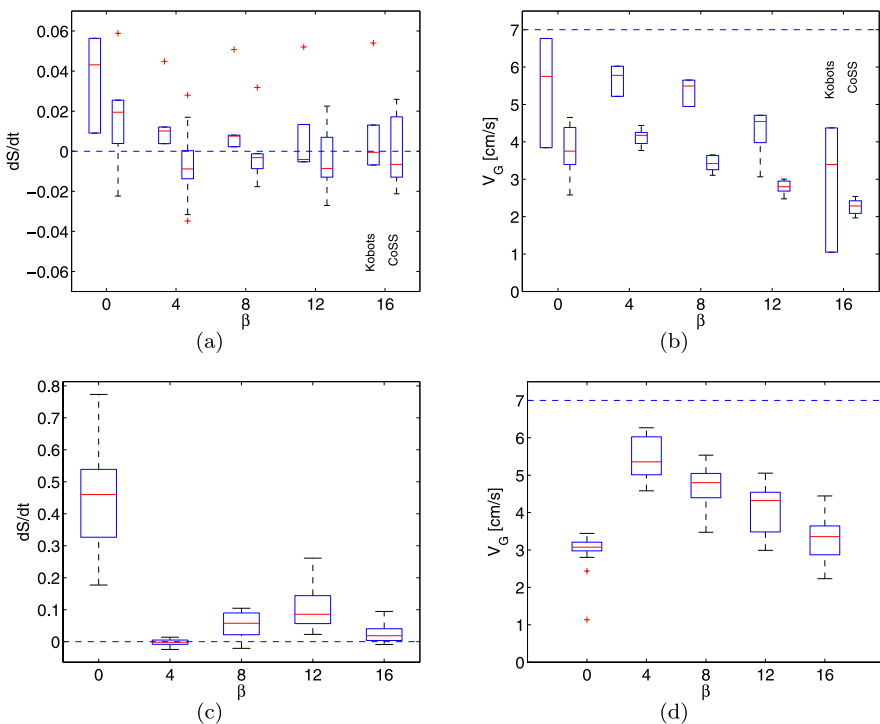Two observations are in order. First, when $\beta = 0$ (meaning that there is no proximal control

Fig. 9 Weight of the proximal control vector (β) experiments. The *upper plots* present the results of the 7
robot experiments in CoSS and Kobots: (**a**) Box-plot of the rate of change of entropy. (**b**) Box-plot of the
swarm velocity. The *lower plots* present the results of the 100 robot experiments in CoSS: (**c**) Box-plot of the
rate of change of the entropy. (**d**) Box-plot of the swarm velocity. The *dashed lines* in (**b**) and (**d**) indicate
the value of the maximum forward velocity $u_{max} = 7$ cm/s. $dS/dt = 0$ is indicated by the *dashed lines* in (**a**)
and (**c**). In this and subsequent box-plot figures, '+' signs denote the outliers

to keep the coherence of the group), dS/dt is maximally positive indicating that the robots are spreading apart in time. Second, as β gets larger, the swarm gets slower. This is due to the fact that as the proximal control becomes stronger, the order of the swarm tends to be smaller, and therefore the average velocity of the robots tend to be reduced due to forward speed modulation. The swarm velocities obtained with $\beta = 0$ are not included, since the robots no longer form a coherent group in this case.

An analysis of Figs. 9(a) and 9(b) shows that the value of β that ensures coherence in groups of 7 robots (simulated or physical) with the largest swarm velocity is 12. However, a similar analysis for 100 simulated robots yields a different optimal value of β as 4, Figs. 9(c) and 9(d). Although the experimental results indicate some discrepancies between physical and simulated Kobots, such as higher swarm velocities in Kobots, the overall dynamics is very similar. The difference in the optimum β values for small and large swarms is an interesting result that needs further investigation.

In the rest of the experiments, we only present the results obtained from the simulation of large swarms since our experiments conducted with small swarms of physical and simulated robots yielded the same optimal parameter values that are obtained with large swarms.

6.2 Proportional gain

The proportional gain (K_p) parameter determines how fast the robots should respond to the 'urge' to turn. We vary K_p (0.1, 0.5 and 0.9) and measure the rate of change of the entropy and swarm velocity for 100 robots in CoSS, as shown in Figs. 10(a) and 10(b), respectively.

It is observed in Fig. 10(a) that dS/dt has a peak when K_p is 0.1 and has values very close to zero for K_p values of 0.5 and 0.9. V_G has its highest value when K_p is equal to 0.1, and decreases with increasing K_p, as shown in Fig. 10(b). The order of the swarm (graph not shown) is maintained for all of the values of K_p and its settling time decreases for high values of K_p. The best value of K_p is 0.5 since the swarm remains coherent and has a moderate swarm velocity.

6.3 Maximum forward speed

We vary $u_{\max}$ and measure the rate of change of entropy and swarm velocity for 100 robots in CoSS and plot the results in Figs. 11(a) and 11(b), respectively.
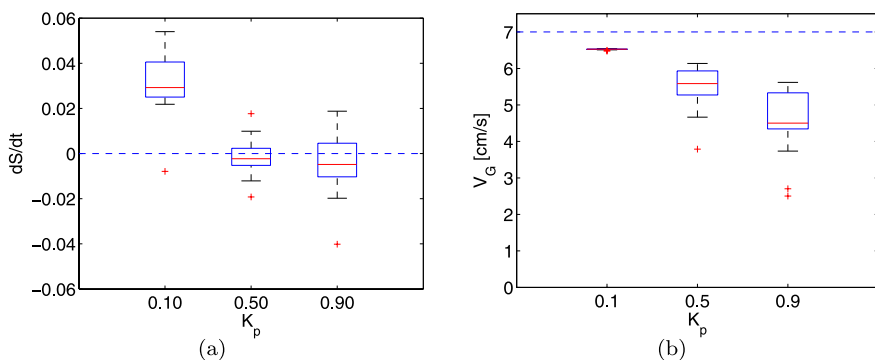

Fig. 10 Proportional gain (K_p) experiments. (**a**) Box-plot of the rate of change of entropy at the end of the experiments. (**b**) Box-plot of the swarm velocity
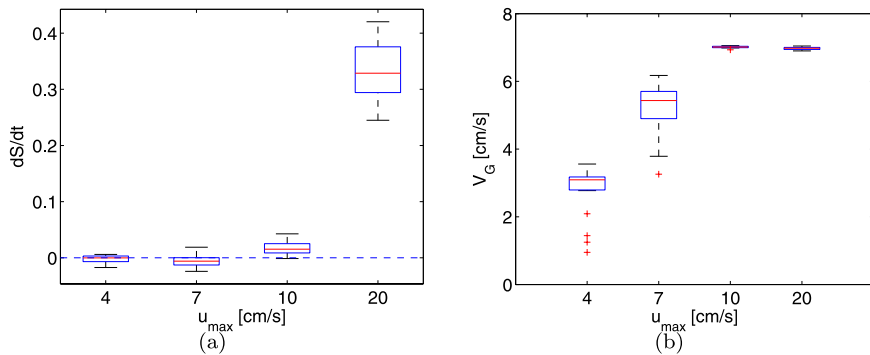
Fig. 11 Maximum forward velocity (u_{max}) experiments. (**a**) Box-plot of the rate of change of entropy at the end of the experiments. (**b**) Box-plot of the swarm velocity
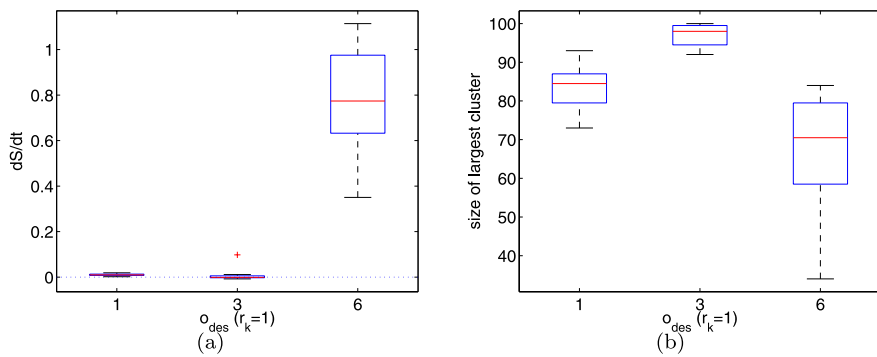

Fig. 12 Desired detection level for robots (o_{des} for $r_k = 1$) experiments. (**a**) Box-plot of the rate of change of entropy at the end of the experiments. (**b**) Box-plot of the size of largest cluster

It is observed in Fig. 11(a) that dS/dt is approximately zero for all the tested values of $u_{max} \leq 10$ cm/s. V_G increases when u_{max} is increased, reaching the value of 7 cm/s for $u_{max} \geq 10$ cm/s. The order reaches a very high value for all of the tested values of u_{max} (graph not shown). The best value of u_{max} is therefore 7 cm/s since the coherence of the swarm is preserved and V_G reaches a reasonably high value.

6.4 Desired detection level for robots

The desired detection level (o_{des}) is the output of the IR sensor when the inter-robot distance is at the desired level. We vary o_{des} (1, 3, and 6) and measure the rate of change of entropy and the size of the largest cluster for 100 robots in CoSS. The results are plotted in Figs. 12(a) and 12(b), respectively.

The choice of $o_{des} = 3$ is the best among the three alternatives. In this case, dS/dt remains close to zero (see Fig. 12(a)) and the size of the largest cluster is approximately 100 (see Fig. 12(b)), which indicates that cohesion of the swarm is maintained.
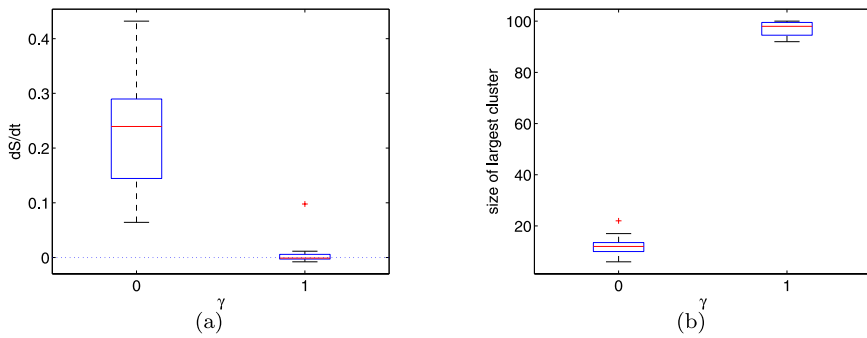
Fig. 13 Modulation of forward velocity (γ) experiments. (**a**) Box-plot of the rate of change of entropy at the end of the experiments. (**b**) Box-plot of the size of the largest cluster
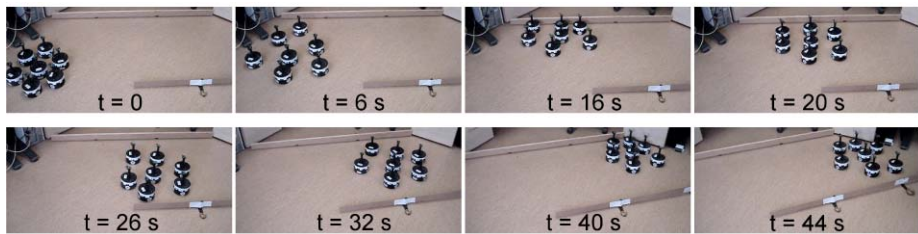

Fig. 14 Self-organized flocking with seven Kobots. Starting from a connected but unaligned state, Kobots negotiate a common heading and move as a group in a constrained environment and bounce off a wall without losing their cohesion

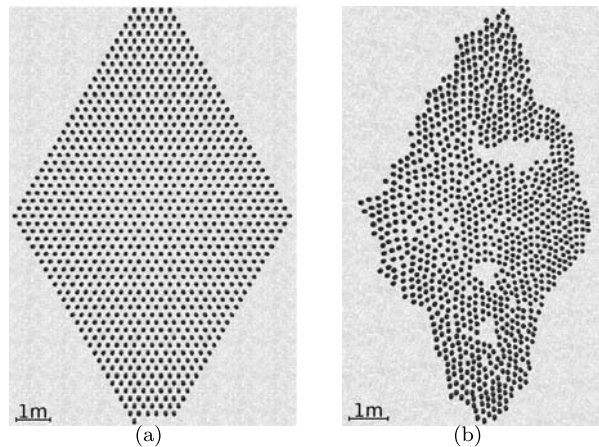6.5 Modulation of forward velocity

The γ parameter determines whether the forward velocity of the robot is modulated or not. When γ is equal to 1, the modulation is enabled; and when γ is equal to 0, the modulation is disabled. We set γ to be either 0 or 1, and measure the rate of change of entropy and the size of the largest cluster for 100 robots in CoSS to investigate the effect of γ on the flocking behavior. The results are plotted in Figs. 13(a) and 13(b), respectively.

It is observed in Fig. 13(a) that dS/dt is positive for $\gamma = 0$, indicating a loss of coherence of the swarm, while it is approximately zero for $\gamma = 1$. The same result is also evident in Fig. 13(b) which shows that the size of the largest cluster when $\gamma = 0$ is approximately 10 robots instead of being 100. The reason behind this failure, when $\gamma = 0$, is the inability of the robots to modulate their forward velocity, which eventually leads to collisions among the robots.

7 Flocking in Kobots and in CoSS

The flocking behavior, as implemented on Kobots using the default parameter settings given in Table 1, is demonstrated in a closed arena, as shown in Fig. 14. Seven robots initially positioned in random orientations and connected via proximal sensing are allowed to move in an environment with a narrow passage. At time $t = 0$, the robots start from a highly

Fig. 15 Open-space flocking
with a large swarm. (**a**) The
screenshot at the beginning of the
simulation. (**b**) The screenshot
when $t = 2000$ s. The total
displacement of the swarm is
approximately 110 m

disordered, but proximally connected configuration having a low order and a low entropy
value. Due to the modulation, the forward velocity of the robots becomes minimal, making
the robots mostly turn in place, aligning themselves with the rest of the swarm. We call
this in-place rotation phase the *alignment* phase. At its end, the swarm is highly aligned
and it begins moving forward. We call this new phase the *advance* phase. When the swarm
meets the wall ($t = 6$ s), the robots in the front sense the wall, slow down and turn to avoid
it. The rest of the swarm also slows down and starts turning in order to avoid the already
stopped/turning robots. In this phase, which we call the *avoidance* phase, the order in the
swarm decreases ($t = 16$ s). The swarm, after successfully avoiding the wall, aligns in a
different direction, away from the obstacle. When the order is restored, the swarm returns to
the *advance* phase ($t = 20$ s). As can be seen in Fig. 14, the 7-robot swarm further encounters
other walls in the environment, successfully demonstrating wall avoidance ($t = 26$ s and
$t = 40$ s). After each of these encounters, the swarm restores its order ($t = 32$ s and $t = 44$ s)
and continues to move. We refer the reader to our previous work (Turgut et al. 2008) for a
more detailed analysis of the dynamics in the different phases of flocking in Kobots. A video
recording of a Kobot swarm moving in a closed arena as a flock is available in the online
supplementary material: Self-organized-flocking.

In order to demonstrate the scalability of the flocking behavior in open space, we also
simulate 1000 robots in CoSS. In this experiment, the robots are initially placed in a regular
hexagonal formation with random orientations as shown in Fig. 15(a). The robots are left
to move for 2000 s after which they end up in the formation shown in Fig. 15(b), which
indicates that robust and scalable flocking is attained with the default parameters. It should
be noted, however, that the scalability demonstrated by this experiments is mainly concerned
with the *alignment* and *advance* phases of the behavior, and does not necessarily imply
scalability in the *avoidance* phase. This is an issue that remains to be addressed in further
studies.

8 Analysis of flocking behavior under different VHS characteristics

The performance of the flocking behavior is mainly determined by the characteristics of the
VHS. In this section, we evaluate the performance of the flocking in open environments in
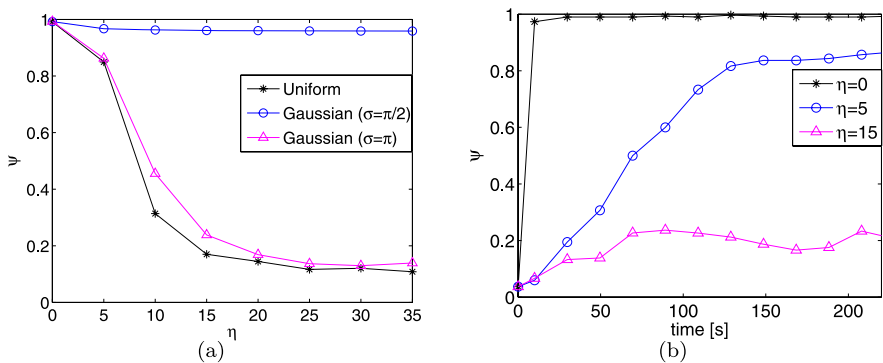large swarms by varying: (1) the nature (ξ_o) and the amount (η) of the noise of the digital

Fig. 16 Noise experiments. Plot of the order. (**a**) The steady-state response as a function of η. (**b**) The transient response as a function of time

compass, (2) the number of VHS neighbors (N_c), and (3) the range of wireless communication (R).

We conduct the experiments using 100 simulated robots. The robots, initially placed in a regular hexagonal formation with a 25 cm inter-robot spacing and at random orientations, are left to move for 1000 seconds. The experiments are repeated 20 times for each parameter.

8.1 Noise

In Sect. 3.2, we pointed out that the environmental disturbances in the heading measurement, which are modeled as noise, can be quite large. Therefore, we have to investigate how the nature and amount of noise affects flocking. Two sets of experiments are conducted to analyze these two factors. In these experiments, unless otherwise stated, the default parameter values listed in Table 1 are used. As will be shown in Sect. 8.2, the robustness of flocking is greatly enhanced with large N_c values. Therefore, in order to accentuate the effect of noise, we set the number of VHS neighbors to 1.

Nature of noise

We evaluate three different distributions of noise for ξ_o, namely: (1) Gaussian distribution with $\sigma = \pm\infty$ leading to a uniform distribution, (2) Gaussian distribution with $\sigma = \pm\pi$, and (3) Gaussian distribution with $\sigma = \pm\frac{\pi}{2}$. For each distribution, we vary η and measure the steady-state values of order.

The results are plotted in Fig. 16(a). When the noise is assumed to have Gaussian distribution of $\sigma = \pm\frac{\pi}{2}$, the swarm remains ordered for all of the tested η values. However, when the noise is assumed to have a uniform distribution or a Gaussian distribution with $\sigma = \pm\pi$, the swarm is observed to reach an ordered state only for η values smaller than 5.

Amount of noise

We vary the amount of noise and measure the time evolution of order attained by the swarm. In order to accentuate the effect of noise on flocking, we assume that the noise has a uniform distribution. It is observed in Fig. 16(b) that, when η is equal to 0, the swarm rapidly converges to an ordered state. As η increases, the rate of convergence decreases, preventing the swarm to reach an ordered state when $\eta = 15$.
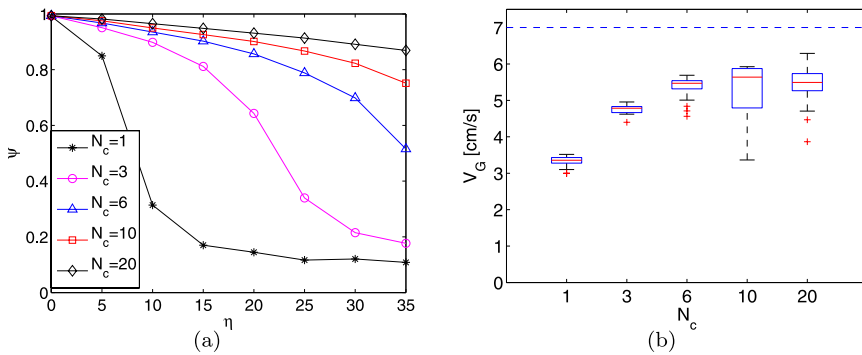
Fig. 17 Number of VHS neighbors (N_c) experiment. (**a**) Plot of the steady-state value of the order. (**b**) Box-plot of the swarm velocity. The *dashed line* indicates the maximum forward velocity

8.2 Number of VHS neighbors

The number of VHS neighbors of the robots is prone to variations depending on the environmental conditions. Therefore, in this section, we vary the number of VHS neighbors and measure the order and the swarm velocity. The noise is assumed to have a uniform distribution in order to accentuate the effect of N_c in the experiments.

Figure 17(a) shows that for small N_c values, the swarm becomes disordered even for small values of η. However, as N_c increases, the swarm remains ordered for larger values of η. An η value of 15 makes the swarm disordered when N_c is equal to 1. However, when N_c is equal to 10, the swarm is ordered at this η value. In the extreme case when N_c is equal to 20, order remains at approximately 0.9 even for an η of 35. In Fig. 17(b) we observe a similar trend for V_G. V_G increases monotonically as N_c increases, approaching asymptotically 6 cm/s. Similar dynamics are also observed in the experiments conducted with Kobots. We conclude that the robustness of the system to sensing noise is highly dependent on the number of VHS neighbors and it is favorable to have as many neighbors as possible.

8.3 The range of the wireless module

The range of the wireless module (R) determines the maximum range of communication of the VHS which is the maximum possible distance to the farthest VHS neighbor. In that sense, R has an effect on the number of VHS neighbors of a robot. We vary the range of communication of VHS and measure the rate of change of entropy and the size of the largest cluster during the last 500 seconds of the simulations for 100 robots in CoSS. We set R to 0.4, 1.0 and 2.0 m. When $R = 0.4$ m, the VHS sensing is local, since not every robot in the swarm is within the communication range of every other robot. However, when $R = 2.0$ m, every robot is in the sensing range of all the others, hence the VHS sensing is global. $R = 1.0$ m is an intermediate value, for which VHS sensing is neither global nor local. The number of VHS neighbors is taken as the mean values obtained in Prowler experiments, shown in Fig. 4(b) in Sect. 3.2, which is 5 for 0.4 m, 25 for 1 m, and 20 for 2 m. The results of the experiment are plotted in Figs. 18(a) and 18(b).

In Fig. 18(a), it can be observed that when the range is 0.4 m, dS/dt is positive, meaning that the swarm is not able to remain coherent. When the range is increased to 1.0 or 2.0 m, dS/dt is approximately 0, indicating a coherent swarm. Similar results are also observed in Fig. 18(b). A cluster size of 100 robots is only observed when the range is greater than
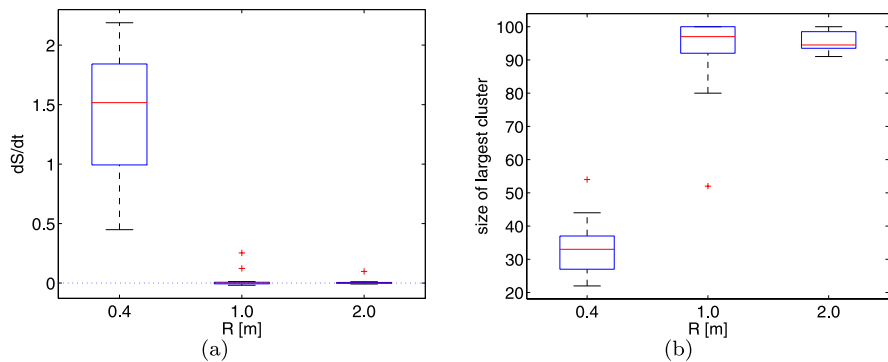
Fig. 18 The range of wireless communication (R) experiments. (**a**) Box-plot of the rate of change of entropy. (**b**) Box-plot of the size of the largest cluster

1.0 m. For a range of 0.4 m, the swarm separates into independently moving clusters (2–4 clusters) causing a decrease in the number of robots in the largest cluster.

As a conclusion, we can say that an aligned and coherent motion is only possible when the range of communication tends to be global. We do not consider this as a limitation since the range of VHS is 20 m in indoor environments which is sufficient to cover thousands of robots.

9 Discussion

The experimental results presented in the previous section show that the flocking behavior proposed is robust against the number of VHS neighbors and the size and nature of noise in heading measurements. The experiments also indicate that the wireless communication range is the main parameter that determines the maximum size a swarm can have and still be able to flock as a single swarm. We observed that swarms that spread wider than the communication range tend to split into smaller swarms. This is an interesting result that needs further investigation, and needs to be discussed with respect both to flocking in nature and to theoretical results from statistical physics and control theory.

Our results show that the swarm fails to adopt a common heading when the range of communication is local. This result is in fact in accordance with the theorem proven by Mermin and Wagner in 1966. In their study, Mermin and Wagner studied phase transitions in materials. They proved that:

"... at any nonzero temperature, a one- or two- dimensional isotropic spin-S Heisenberg model with finite range of interaction can be neither ferromagnetic or antiferromagnetic" (Mermin and Wagner 1966).

This means that, in 1-D and 2-D systems, the system cannot attain a long-range order using only short-range interactions if there is any noise in the system. It has been shown that random errors made at each step are accumulated at exactly the same rate as they disperse in 1-D or 2-D.

In a later study, Vicsek developed the Self-Driven Particles (SDP) model showing that mobile (though massless and volumeless) particles can attain a common heading in 1-D and 2-D using only short-range interactions despite the existence of noise, contradicting the

claims of Mermin–Wagner theorem. This apparent contradiction was later resolved by Toner and Tu (1998) who showed that the mobility of the particles in Vicsek's model, in contrast to the immobility of particles in Mermin–Wagner's model, made the difference. They claimed that, in the SDP model, the neighbors of particles tended to change in time, and that these changes created pseudo-long-range interactions in the system leading to long-range order.

In a recent follow-up to this discussion, Aldana and Huepe (2003) studied the transition to long-range order in a system of immobile particles, similar to the one considered by Mermin and Wagner. They assumed that each particle has a certain number of neighbors, which are chosen with probability p from the local neighborhood, and with probability $1-p$ randomly from all particles. Although the particles are stationary, this parameter enables the amount of long-range connections within the system to be determined. With $p = 0$, the interactions are totally random, while with $p = 1$ the system reduces to the model that was considered by Mermin–Wagner with stationary particles and finite range interactions. They reported that, in systems with noise, a phase transition to long-range order is still possible even if $p = 0.99$. This result showed that although long-range information is essential to attain long-range order in such systems, the amount of long-range interactions can be quite low.

The flocking behavior we have obtained with robots is in 2-D. Due to the physical embodiment of the robots as well as the short range of proximity sensors, the neighborhood of robots tends to remain constant during flocking, making the system more closely resemble the system considered by Mermin and Wagner, and Aldana and Huepe. In this sense, we believe that our experimental results showing that the flocking occurs even when VHS neighbors are as low as 1 are due to the existence of long-range interactions enabled by VHS. The fact that the wireless communication range is the determining factor of the swarm size is also in accordance with these theoretical findings.

Despite these results, however, in nature it is common to see schools of fish or flocks of birds that contain large numbers of individuals, which are observed to extend beyond the interaction range among individuals. In particular, it is known that migrating fish can create schools that consist of millions of individuals. There may be many factors at work that increase the scaling of the flocks. First, it is known that birds, and possibly fish, can sense the magnetic field of the Earth and use this information to orient themselves (Beason 2005; Wallraff 2005; Wiltschko and Wiltschko 2005). Second, although interactions are usually assumed to remain local, some direct or occasional long-range interactions may exist. For instance, birds use vision in flocking, and they may also track birds that are further in the flock to occasionally make adjustments. We speculate that the use of a common homing direction, or an indirect or occasional long-range interaction can be at work in natural flocks increasing the scale of their flocks.

10 Conclusions

In this paper, we have shown self-organized flocking in a swarm of mobile robots (Turgut et al. 2008). To the best of our knowledge, this is the first successful implementation of self-organized flocking on physical mobile robots, with completely on-board sensing. We have described a novel robot platform (Turgut et al. 2007) and its sensing system that has been essential for this achievement. We have described the flocking behavior based on heading alignment and proximal control behaviors.

In order to investigate the performance of flocking on large numbers of robots (Çelikkanat et al. 2007), we implemented a realistic simulator by systematically modeling the

characteristics of the sensing systems. After verifying it against the physical robots in open-space flocking, we investigated how the different characteristics of relative heading measurements (VHS) affect the performance of flocking. Our results showed that the system is quite robust to large amounts of noise, even when each robot hears from a single neighbor. However, both the robustness against noise and the swarm velocity increase significantly when the number of VHS neighbors increases. We have also shown that the communication range determines the size of the swarm, which is consistent with models of flocking in natural systems (Couzin 2007).

References

Aldana, M., & Huepe, C. (2003). Phase transitions in self-driven many-particle systems and related non-equilibrium models: A network approach. *Journal of Statistical Physics*, *112*(1/2), 135–153.

Balch, T. (2000). Hierarchic social entropy: An information theoretic measure of robot group diversity. *Autonomous Robots*, *8*(3), 209–237.

Baldassarre, G. (2008). Self-organization as phase transition in decentralized groups of robots: A study based on Boltzmann entropy. In P. Mikhail (Ed.), *Advances in applied self-organizing systems* (pp. 127–146). Berlin: Springer.

Ballerini, M., Cabibbo, N., Candelier, R., Cavagna, A., Cisbani, E., Giardina, I., Lecomte, V., Orlandi, A., Parisi, G., Procaccini, A., Viale, M., & Zdravkovic, V. (2008). Interaction ruling animal collective behavior depends on topological rather than metric distance: Evidence from a field study. *Proceedings of the National Academy of Sciences*, *105*(4), 1232–1237.

Beason, R. C. (2005). Mechanisms of magnetic orientation in birds. *Integrative and Comparative Biology*, *45*(3), 565–573.

Camazine, S., Deneubourg, J.-L., Franks, N. R., Sneyd, J., Theraulaz, G., & Bonabeau, E. (2001). *Self-Organization in Biological Systems*. New Jersey: Princeton University Press.

Campo, A., Nouyan, S., Birattari, M., Groß, R., & Dorigo, M. (2006). Negotiation of goal direction for cooperative transport. In M. Dorigo et al. (Eds.), *Lecture notes in computer science: Vol. 4150. Ant colony optimization and swarm intelligence: 5th international workshop*, ANTS 2006 (pp. 191–202). Berlin: Springer.

Çelikkanat, H., Turgut, A. E., Gökçe, F., & Şahin, E. (2007). *Evaluation of robustness in self-organized flocking* (Tech. Rep. METU-CENG-TR-2008-02). Dept. of Computer Eng., Middle East Tech. Univ., Ankara, Turkey.

Correll, N., Sempo, G., de Meneses, Y. L., Halloy, J., Deneubourg, J.-L., & Martinoli, A. (2006). SwisTrack: A tracking tool for multi-unit robotic and biological systems. In *Proceedings of the IEEE/RSJ international conference on intelligent robots and systems* (pp. 2185–2191). New Jersey: IEEE Press.

Couzin, I. (2007). Collective minds. *Nature*, *445*, 715.

Dalgaard, P. (2004). *Introductory statistics with R*, 3rd edn. *Statistics and computing*. New York: Springer.

Gregoire, G., Chate, H., & Tu, Y. (2003). Moving and staying together without a leader. *Physica D*, *181*, 157–170.

Hayes, A., & Dormiani-Tabatabaei, P. (2002). Self-organized flocking with agent failure: Off-line optimization and demonstration with real robots. In *Proceedings of the IEEE international conference on robotics and automation* (pp. 3900–3905). New Jersey: IEEE Press.

Kelly, I., & Keating, D. (1996). Flocking by the fusion of sonar and active infrared sensors on physical autonomous robots. In *Proceedings of the third international conference on mechatronics and machine vision in practice* (Vol. 1, pp. 14–17). Guimarães: Universidade do Minho.

Kruszelnicki, K. S. (2008). Physics of flocks. http://www.abc.net.au/science/k2/moments/gmis9845.htm.

Mataric, M. J. (1994). Interaction and intelligent behavior. Ph.D. thesis, MIT.

Mermin, N. D., & Wagner, H. (1966). Absence of ferromagnetism or antiferromagnetism in one or two-dimensional isotropic Heisenberg models. *Physical Review Letters*, *17*(22), 1133–1136.

Miglino, O., Lund, H. H., & Nolfi, S. (1995). Evolving mobile robots in simulated and real environments. *Artificial Life*, *2*(4), 417–434.

Moshtagh, N., Jadbabaie, A., & Daniilidis, K. (2006). Vision-based control laws for distributed flocking of nonholonomic agents. In *Proceedings of the IEEE international conference on robotics and automation* (pp. 2769–2774). New Jersey: IEEE Press.

Nembrini, J. (2005). Minimalist coherent swarming of wireless networked autonomous mobile robots.

Nembrini, J., Winfield, A. F. T., & Melhuish, C. (2002). Minimalist coherent swarming of wireless networked autonomous mobile robots. In B. Hallam, D. Floreno, J. Hallam, G. Hayes, & J.-A. Meyer (Eds.), *Proceedings of the 7th international conference on the simulation of adaptive behavior conference* (Vol. 7, pp. 273–382). Cambridge: MIT Press.

Okubo, A. (1986). Dynamical aspects of animal grouping: Swarms, schools, flocks, and herds. *Advances in Biophysics*, *22*, 1–94.

Parrish, J. K., Viscido, S. V., & Grünbaum, D. (2002). Self-organized fish schools: An examination of emergent properties. *The Biological Bulletin*, *202*, 296–305.

Partridge, B. (1982). The structure and function of fish schools. *Scientific American*, *246*, 114–123.

Pitcher, T. J., & Parrish, J. K. (1993). Functions of shoaling behavior in teleosts. In T. J. Pitcher (Ed.), *Behaviour of teleost fishes* (pp. 363–439). London: Chapman and Hall.

Regmi, A., Sandoval, R., Byrne, R., Tanner, H., & Abdallah, C. (2005). Experimental implementation of flocking algorithms in wheeled mobile robots. In *Proceedings of American control conference* (Vol. 7, pp. 4917–4922). New Jersey: IEEE Press.

Reynolds, C. (1987). Flocks, herds and schools: A distributed behavioral model. In *Proceedings of the 14th annual conference on computer graphics and interactive techniques (SIGGRAPH '87)* (pp. 25–34). New York: ACM Press.

Simon, G., Volgyesi, P., Maroti, M., & Ledeczi, A. (2003). Simulation-based optimization of communication protocols for large-scale wireless sensor networks. In *IEEE aerospace conference* (Vol. 3, pp. 1339–1346). New Jersey: IEEE Press.

Simons, A. M. (2004). Many wrongs: the advantage of group navigation. *Trends in Ecology & Evolution*, *19*(9), 453–455.

Simpson, S. J., Sword, G. A., Lorch, P. D., & Couzin, I. D. (2006). Cannibal crickets on a forced march for protein and salt. *Proceedings of the National Academy of Sciences*, *103*(11), 4152–4156.

Toner, J., & Tu, Y. (1998). Flocks, herds, and schools: A quantitative theory of flocking. *Physical Review E*, *58*, 4828–4858.

Turgut, A. E., Gökçe, F., Çelikkanat, H., Bayındır, L., & Şahin, E. (2007). *Kobot: A mobile robot designed specifically for swarm robotics research* (Tech. Rep. METU-CENG-TR-2007-05). Dept. of Computer Eng., Middle East Tech. Univ., Ankara, Turkey.

Turgut, A. E., Çelikkanat, H., Gökçe, F., & Şahin, E. (2008). Self-organized flocking with a mobile robot swarm. In: *Proceedings of the 7th international conference on autonomous agents and multiagent systems*, AAMAS 2008 (pp. 39–46). International Foundation for Autonomous Agents and Multiagent Systems.

Vicsek, T., Czirók, A., Ben-Jacob, E., Cohen, I., & Shochet, O. (1995). Novel type of phase transition in a system of self-driven particles. *Physical Review Letters*, *75*(6), 1226–1229.

Wallraff, H. G. (2005). *Avian navigation: Pigeon homing as a paradigm*. Berlin: Springer.

Wiltschko, W., & Wiltschko, R. (2005). Magnetic orientation and magnetoreception in birds and other animals. *Journal of Comparative Physiology A: Neuroethology, Sensory, Neural, and Behavioral Physiology*, *191*(8), 675–693.